

# Validation of Aerosol Dynamics in a Well-Stirred Isothermal Enclosure

Amy Mensch, Thomas Cleary

*National Institute of Standards and Technology, Gaithersburg, MD, USA*

## Abstract

Modeling of aerosol dynamics in fire simulations enables predictions of the effects of soot, such as visibility and detection, and the fate of soot, such as deposition and emissions. NIST's fire modeling tool, Fire Dynamics Simulator (FDS) [1], has implemented computational schemes for aerosol transport, deposition and coagulation [2]–[4]. Users rely on FDS's aerosol dynamics sub-models to make predictions of smoke detection, visibility, tenability, deposition on surfaces for fire forensics, and smoke control for abatement. This study presents measurements from experiments in a well-stirred, isothermal enclosure using spherical aerosol particles across a range of initial aerosol conditions and fan flow settings. The measured reductions in particle number concentration are represented by a decay constant for each experiment. These results are compared to FDS predictions, and the sources of differences between the measurements and predictions are discussed.

**Keywords:** soot deposition, soot modeling, aerosol coagulation, aerosol deposition

## Introduction

Surface deposition occurs when particles come in contact with surfaces and are removed from the flow. Coagulation of aerosol particles occurs when particles collide with each other due to their relative motion and combine to create a larger particle. Both deposition and coagulation of aerosol occur due to multiple transport mechanisms, including gravitational settling, Brownian diffusion and turbulent diffusion. Surface deposition in a fire environment is also caused by thermophoresis, driven by temperature gradients in the gas. FDS treats aerosol transport like other gaseous species, but applies additional, independent deposition velocities for gravitational, turbulent and thermophoretic deposition. Brownian diffusion losses are less important in typical fire scenarios, and the calculated turbulent deposition velocity combines both Brownian and

turbulent diffusion into one term [5]. Particle coagulation can also be calculated by FDS when size bins are defined for the aerosol species. The coagulation mechanisms in FDS are Brownian, gravitational, shear, and inertial [5].

Previous fire experiments measuring soot deposition [6], [7] included contributions from gravitational, thermophoretic, and turbulent deposition and from coagulation, making it difficult to use these results to understand any specific mechanism. The thermophoretic deposition equations in FDS were previously validated for soot in laminar flow channel experiments with opposing hot and cold surfaces by Mensch and Cleary [8]. The effect of aerosol coagulation was demonstrated by Rexfort [9], who computed soot number concentration for a standard heptane fire (EN 54 part 9 [10]) based on aerosol concentration predictions from a previous version of FDS without coagulation or deposition. When Rexfort included coagulation, the agreement with the measured number concentration improved, particularly after the fire was extinguished.

This study focuses on the gravitational and turbulent deposition as well as coagulation in isothermal experiments in a well-stirred, isothermal enclosure with a fan in the center that directs flow upward similar to a buoyant plume from a fire. The turbulent deposition models in FDS were developed from fully-developed turbulent channel experiments and need to be verified for turbulent plume flow. Although soot produced from flaming fires is generally characterized as a fractal structure, FDS's deposition and coagulation routines are based on well-established correlations for spherical particles. The experiments in this study are limited to spherical particles of known size distribution to validate the aerosol dynamics routines currently in FDS with an extension to fractal soot particles to be conducted in a future study.

## **Experimental Methods**

A diagram of the  $\sim 1.5 \text{ m}^3$  isothermal aluminium enclosure used in the experiments is shown in Fig. 1(a). Experiments were conducted at four different fan speeds with flow rates of  $0.0085 \text{ m}^3/\text{s}$ ,  $0.018 \text{ m}^3/\text{s}$ ,  $0.029 \text{ m}^3/\text{s}$  and  $0.051 \text{ m}^3/\text{s}$ . The flows were estimated from the fan specification of flow at maximum rotational speed and the relationship between fan rotational speed and the flow. The normalized velocity distribution just above the fan was characterized with a velocity probe in a  $0.02 \text{ m} \times 0.02 \text{ m}$  grid (36 total measurements). The maximum velocities were  $1 \text{ m/s}$ ,  $2 \text{ m/s}$ ,  $3.3 \text{ m/s}$  and  $6 \text{ m/s}$  for the four fan settings used to produce the nominal fan flow rates. Monodisperse spherical aerosol particles were generated by condensing di-ethyl-hexyl-sebacat on solid seed particles in a condensation monodisperse aerosol generator. Five size distributions with count-median diameters of  $0.18 \text{ }\mu\text{m}$ ,  $0.38 \text{ }\mu\text{m}$ ,  $0.53 \text{ }\mu\text{m}$ ,  $0.96 \text{ }\mu\text{m}$ , and  $1.77 \text{ }\mu\text{m}$  were examined. The aerosol was passed through a charge neutralizer, then introduced into the enclosure through

the “inlet” until the desired number concentration was reached, either  $1.0 \text{ E}10 /\text{m}^3$ ,  $4.0 \text{ E}10 /\text{m}^3$ ,  $1.6 \text{ E}11 /\text{m}^3$ , or  $6.4 \text{ E}11 /\text{m}^3$ .

Aerosol was sampled from the enclosure to measure the initial size distribution with an electrical low-pressure impactor. Then, a sample was continuously withdrawn at  $5 \text{ E-}6 \text{ m}^3/\text{s}$  ( $0.3 \text{ L}/\text{min}$ ) to a condensation particle counter to measure the number concentration at a rate of  $1 \text{ Hz}$ . Filtered and humidified make-up air was introduced through the inlet at a flow of  $8.3 \text{ E-}6 \text{ m}^3/\text{s}$  ( $0.5 \text{ L}/\text{min}$ ) to exclude ambient particle-laden air from infiltrating the enclosure. Due to wall losses, coagulation, and sampling, the number concentration decayed over the observation time of  $1000 \text{ s}$ . The observation time started when the initial number concentration was reached. At the end of the observation time, the final aerosol size distribution was recorded. The measured geometric mean diameter was the same or larger at the end of the observation time, with larger increases occurring with higher initial number concentration, as expected. The results are not presented due to space limitations.

### Computational Modeling

A difficulty in modeling aerosol dynamics of non-spherical particles is defining the appropriate characteristic size(s) to represent multiple real particle phenomena. Aerosol size can be characterized by various measurement techniques, and a single characterization is not appropriate for all soot phenomena. For example, characteristic size can be determined according to mobility, inertial drag, coagulation, light scattering, or thermophoresis. Additionally, the numerical representation of any size distribution must be limited by the number of size bins. Too few bins will lead to inaccurate results; too many will be computationally inefficient. For each nominal particle size, eight bin sizes were used to represent the size distribution, with different bin widths for each nominal size, covering at least a decade in size and including larger size bins for particle growth. Five log-normal size distributions in Table 1, representing the typical experimental size distributions, were specified in FDS.

Table 1. Log-Normal Particle Size Distributions and Bin Sizes

Geometric mean diameter ( $\mu\text{m}$ )	0.18	0.38	0.53	0.96	1.77
Geometric standard deviation	1.60	1.30	1.24	1.28	1.28
Minimum size of FDS bins ( $\mu\text{m}$ )	0.06	0.18	0.3	0.5	0.8
Maximum size of FDS bins ( $\mu\text{m}$ )	2	2.5	3	4	5

A series of simulations were run to examine the effects of grid resolution on the predictions of aerosol number concentration. Uniform rectangular grids were used with  $2.2 \text{ E}4$  cells,  $1.8 \text{ E}5$  cells, and  $1.5 \text{ E}6$  cells, which produced cells with dimensions of  $0.04 \text{ m}$ ,  $0.02 \text{ m}$ , and  $0.01 \text{ m}$ , respectively. Over the particle size distributions examined, the results varied significantly between the  $0.04 \text{ m}$  and  $0.02 \text{ m}$  grid resolutions, with

the 0.04 m grid resolution predicting lower number concentrations at 1000 s. The results for the 0.02 m results and the 0.01 m results were much closer than the 0.04 m results and 0.02 m results. This apparent solution convergence led to the specification of 0.01 m grid dimension ( $1.5 \text{ E}6$  cells) for the simulations presented here.

FDS simulations of the spherical particle coagulation and losses in the enclosure were conducted to compare to the experimental measurements. The vertical boundaries of the cells representing the fan presented additional surface area for deposition. Coagulation was calculated for the eight bin sizes representing the size distribution. Additional cases were run with coagulation turned off for all fan velocities and size distributions. A flow of  $8.3 \text{ E}-6 \text{ m}^3/\text{s}$  (0.5 L/min) was removed from the enclosure through the outlet, and  $8.3 \text{ E}-6 \text{ m}^3/\text{s}$  (0.5 L/min) of clean air entered through the inlet throughout the simulation to represent the sampling and make-up air in the experiment. Initial simulations showed the aerosol was well mixed within a couple of minutes after the injection period.

Figure 1(b) shows the velocity vectors for an example FDS case with a nominal 2 m/s maximum fan velocity. The walls of the enclosure are colored according to the mass of deposition, with most of the deposition occurring on the bottom surface, and some locally higher levels of deposition on the top surface above the fan.

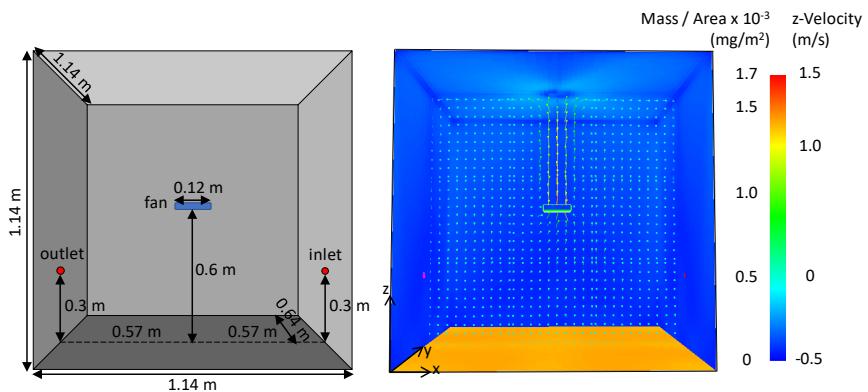


Fig. 1. (a) Diagram of isothermal enclosure and (b) FDS results of surface deposition mass loading and z-velocity vectors with coagulation off,  $1.8 \text{ E}5$  cells (0.02 m cell dimension), a nominal maximum fan speed of 2 m/s, and an initial concentration of  $4.0 \text{ E}10 / \text{m}^3$  particles with a geometric mean diameter of  $0.18 \mu\text{m}$ , at approximately 800 s of deposition time.

## Results and Discussion

The direct measurements gathered during the experiments were of particle number concentration, with the reduction related to both wall

losses and coagulation, whereas mass concentration measurements would relate directly to wall losses alone. The number concentration reduction was approximated as an exponential decay,

$$N/N_o = e^{-at} \quad (\text{Eq. 1})$$

$$a = \alpha + \beta + \gamma \quad (\text{Eq. 2})$$

where  $a$  is the overall decay coefficient and  $\alpha$ ,  $\beta$  and  $\gamma$  are the contributions from dilution, deposition and coagulation. The dilution decay constant is fixed at  $5.6 \text{ E-6 s}^{-1}$  from the make-up flow and enclosure volume. In general, the individual decay coefficients for deposition and coagulation are not constant. However, for the small dilution flow, narrow size distributions, relatively low initial concentrations, and relatively short observation time considered, treating the overall decay coefficient as a constant is a reasonable approximation. Fitting the decay curve to an exponential function over the entire observation time allows for comparison of the results between different fan flows, size distributions and concentrations considered. All the decay constant results presented here (both experimental and simulation) fit an exponential function to a high degree, with correlation coefficients typically higher than 0.99.

Figs. 2-5 show the simulation and experimental results for the four fan flow rates. The simulation results show clearly that the decay constant goes through a minimum around  $0.3 \mu\text{m}$  to  $0.4 \mu\text{m}$  at all concentrations. The decay constant also increases as the number concentration increases. The experimental results show the same trends. The increase in the decay constants from the no coagulation simulations to the simulations for  $1.0 \text{ E}10 / \text{m}^3$  is slight, as expected, as the coagulation rate is a function of the particle concentration. As the fan flow rate increases the decay constants increase somewhat for the simulations. The increase in the decay constants with increasing fan flow is much more pronounced in the experiments, particularly at the two highest flow rates.

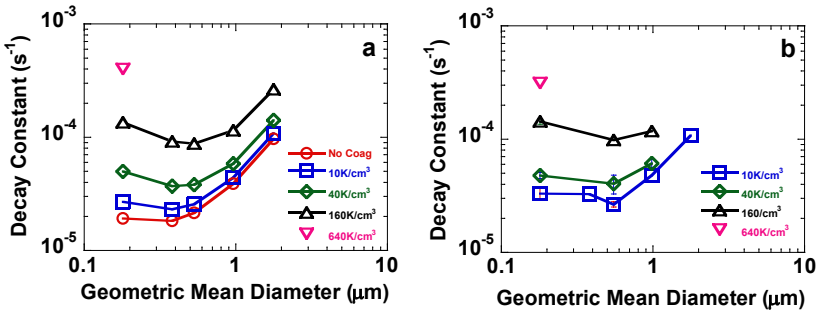


Fig. 2. (a) Simulation results and (b) experimental results the fan flow rate of  $0.0085 \text{ m}^3/\text{s}$  (maximum fan speed  $1 \text{ m/s}$ ).

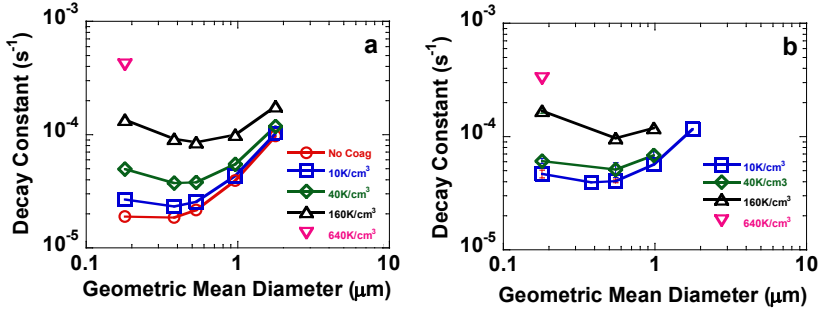


Fig. 3. (a) Simulation results and (b) experimental results for the fan flow rate of 0.018 m<sup>3</sup>/s (maximum fan speed 2 m/s).

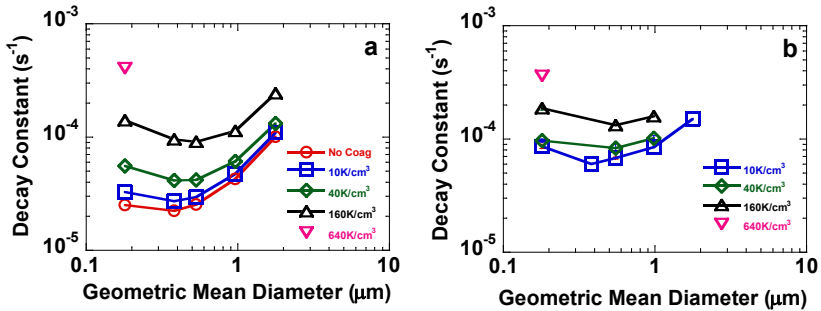


Fig. 4. (a) Simulation results and (b) experimental results for the fan flow rate of 0.029 m<sup>3</sup>/s (maximum fan speed 3.3 m/s).

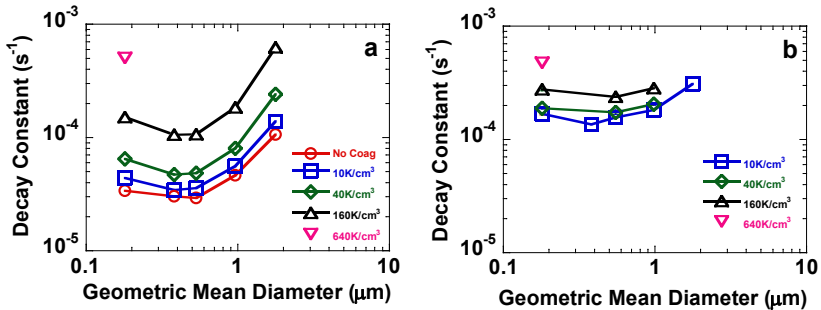


Fig. 5. (a) Simulation results and (b) experimental results for the fan flow rate of 0.051 m<sup>3</sup>/s (maximum fan speed 6 m/s).

The overall comparison between the simulations and experimental results shows better agreement at lower fan flow velocities and at higher particle concentrations. There is no explicit fan particle loss function modeled beyond the surface deposition routine. At the higher particle

concentrations, the change in the number concentration is more due to coagulation than deposition, so any effect of fan flow on losses is less apparent. Increased volumetric flow through the fan accounts for the largest deviations between the simulations and experiments. Therefore, it is hypothesized that the additional particle losses observed in the experiments at higher fan settings are due to the effects of high local velocities in the fan itself.

FDS has a filtering feature that can be applied to the fan flow to remove aerosol particles and account for the assumed fan losses. An empirically derived filter function or filter efficiency is based on the particle aerodynamic diameter and the fan flow rate using the experimental results of the conditions examined. The utility of such filter function is seen when the particles studied are soot agglomerates. With a known aerodynamic size distribution of the soot, wall and fan losses can be accounted for directly. This allows for coagulation simulation based on the appropriate agglomerate diameters for soot.

### **Conclusions and Future Work**

Experiments were conducted to validate the deposition and coagulation routines in FDS for spherical particles. Over the range of particle sizes, concentrations, and fan flow rates studied, the simulation predictions and experiments exhibit the same trends in decay constants, with the predictions and experiments in quantitative agreement for low fan flow rates and high particle concentrations. It is hypothesized that at high fan flow rates, additional particle deposition losses within the fan may be the cause of the under-prediction in the decay constants. This un-modeled deposition can be accounted for in FDS using a filter feature; however the additional fan particle losses need to be confirmed experimentally.

In the future, experiments will be conducted to quantify the concentration of particles deposited on wall surfaces and on the fan itself using fluorescein-tagged aerosols. Simulations will be conducted to study the effect of the number of aerosol bins needed to provide reasonable results for fire safety engineering purposes. Experiments will also be conducted in a specially-constructed, recirculating duct to model and quantify deposition in duct flows at fully-developed turbulent conditions.

The experiments to date and planned in the future are designed to validate the FDS subroutines for spherical particles, and ultimately validate soot coagulation and losses from all mechanisms in smoke flows with suitably modified routines for soot agglomerates.

### **References**

- [1] K. McGrattan, S. Hostikka, R. McDermott, J. Floyd, and M. Vanella, "Fire Dynamics Simulator User's Guide 6th Edition," National Institute of Standards and Technology, Gaithersburg, MD, NIST SP 1019, 2018.

- [2] J. Floyd, K. Overholt, and O. Ezekoye, "Soot Deposition and Gravitational Settling Modeling and the Impact of Particle Size and Agglomeration," *Fire Safety Science*, vol. 11, pp. 376–388, 2014, doi: 10.3801/IAFSS.FSS.11-376.
- [3] J. Floyd and R. McDermott, "Modeling soot deposition using large eddy simulation with a mixture fraction based framework," in *Interflam: Proceedings of the 12th International Conference*, 2010.
- [4] J. Floyd, "A numerical investigation on the impact of modeling aerosol behaviors on the prediction of soot density in a compartment fire," in *Interflam: Proceedings of the 14th International Conference*, 2016, vol. 2, pp. 835–846.
- [5] K. McGrattan, S. Hostikka, R. McDermott, J. Floyd, and M. Vanella, "Fire Dynamics Simulator Technical Reference Guide Volume 1: Mathematical Model," National Institute of Standards and Technology, Gaithersburg, MD, NIST Special Publication 1018–1, 2018.
- [6] S. Riahi and C. Beyler, "Measurement and Prediction of Smoke Deposition from a Fire Against a Wall," *Fire Safety Science*, vol. 10, pp. 641–654, 2011, doi: 10.3801/IAFSS.FSS.10-641.
- [7] W. D. Ciro, E. G. Eddings, and A. F. Sarofim, "Experimental and Numerical Investigation of Transient Soot Buildup on a Cylindrical Container Immersed in a Jet Fuel Pool Fire," *Comb. Sci. and Tech.*, vol. 178, no. 12, pp. 2199–2218, Jun. 2006, doi: 10.1080/00102200600626108.
- [8] A. E. Mensch and T. G. Cleary, "Measurements and predictions of thermophoretic soot deposition," *International Journal of Heat and Mass Transfer*, vol. 143, p. 118444, Nov. 2019, doi: 10.1016/j.ijheatmasstransfer.2019.118444.
- [9] C. Rexfort, "Combination of a fire model and a fire sensor model," in *AUBE '04 Conference Proceedings*, Duisburg, Germany, 2004.
- [10] EN 54 part 9 Components of automatic fire detection systems. Methods of test of sensitivity to fire. 2013.